

Reversible Switch in Charge Storage Enabled by Selective Ion Transport in Solid Electrolyte Interphase

Lei Tao, Joshua A. Russell,[○] Dawei Xia,[○] Bingyuan Ma,[○] Sooyeon Hwang,[○] Zhijie Yang, Anyang Hu, Yuxin Zhang, Poom Sittisomwong, Deyang Yu, Paul A. Deck, Louis A. Madsen, Haibo Huang, Hui Xiong,* Peng Bai,* Kang Xu,* and Feng Lin*



Cite This: <https://doi.org/10.1021/jacs.3c03429>



Read Online

ACCESS |



Metrics & More

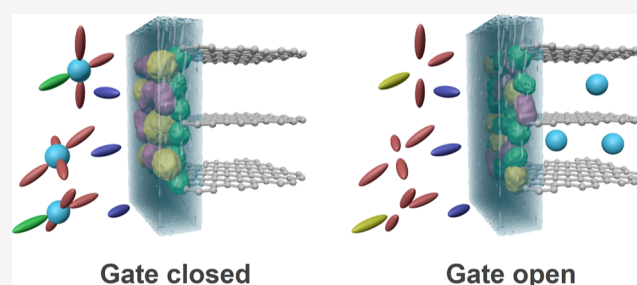


Article Recommendations



Supporting Information

ABSTRACT: Solid–electrolyte interphases (SEIs) in advanced rechargeable batteries ensure reversible electrode reactions at extreme potentials beyond the thermodynamic stability limits of electrolytes by insulating electrons while allowing the transport of working ions. Such selective ion transport occurs naturally in biological cell membranes as a ubiquitous prerequisite of many life processes and a foundation of biodiversity. In addition, cell membranes can selectively open and close the ion channels in response to external stimuli (e.g., electrical, chemical, mechanical, and thermal), giving rise to “gating” mechanisms that help manage intracellular reactions. We wondered whether the chemistry and structure of SEIs can mimic those of cell membranes, such that ion gating can be replicated. That is, can SEIs realize a reversible switching between two electrochemical behaviors, i.e., the ion intercalation chemistry of batteries and the ion adsorption of capacitors? Herein, we report such SEIs that result in thermally activated selective ion transport. The function of open/close gate switches is governed by the chemical and structural dynamics of SEIs under different thermal conditions, with precise behaviors as conducting and insulating interphases that enable battery and capacitive processes within a finite temperature window. Such an ion gating function is synergistically contributed by Arrhenius-activated ion transport and SEI dissolution/regrowth. Following the understanding of this new mechanism, we then develop an electrochemical method to heal the SEI layer in situ. The knowledge acquired in this work reveals the possibility of hitherto unknown biomimetic properties of SEIs, which will guide us to leverage such complexities to design better SEIs for future battery chemistries.



INTRODUCTION

To maximize the energy density output, advanced batteries must operate at extreme voltages where no known electrolyte is thermodynamically stable.^{1–3} The reversibility of such battery chemistry, typically represented by lithium-ion batteries (LIBs), is realized via kinetic stability provided by a nanometric phase formed between electrode and electrolyte called the solid–electrolyte interphase (SEI), which arises from irreversible reactions during the initial cell activation.^{4–7} Since the commercialization of LIBs in the early 1990s,^{3,8} significant research progress has been made in understanding and designing the chemistries, structures, and morphology of SEIs for better performance.^{9–13} SEIs have a stratified structure consisting of a porous organic outer layer and a dense inorganic inner layer that is directly interfaced to the electrode.^{14–17} Most of these chemical components come from the decomposition of electrolyte solvents and salts. These ingredients (oxides, carbonates, semi-carbonates, or fluorides) form a composite and independent phase that conducts the working ion,^{18–20} so that the cell reaction could be sustained, while insulating electrons so that continuous decomposition of

electrolyte components is prevented.^{21,22} Despite the knowledge achieved in the past three decades, the SEI remains to be the least understood component in advanced batteries, with many key questions unanswered,⁶ even while emerging electrode chemistries present new demands and challenges for the SEIs.

Recent advances achieved with new analytical tools have led to key findings about SEIs, such as hitherto unknown SEI components, their dynamic nature and evolution during the long-term exposure to battery environment, and the tailoring of SEI chemistry and properties via electrolyte engineering.^{23–28} The solvation structure of the working ion and fluorination of the solvent molecules are the most popular tools in guiding the formation of SEIs.^{29,30} The traditional SEI

Received: April 2, 2023

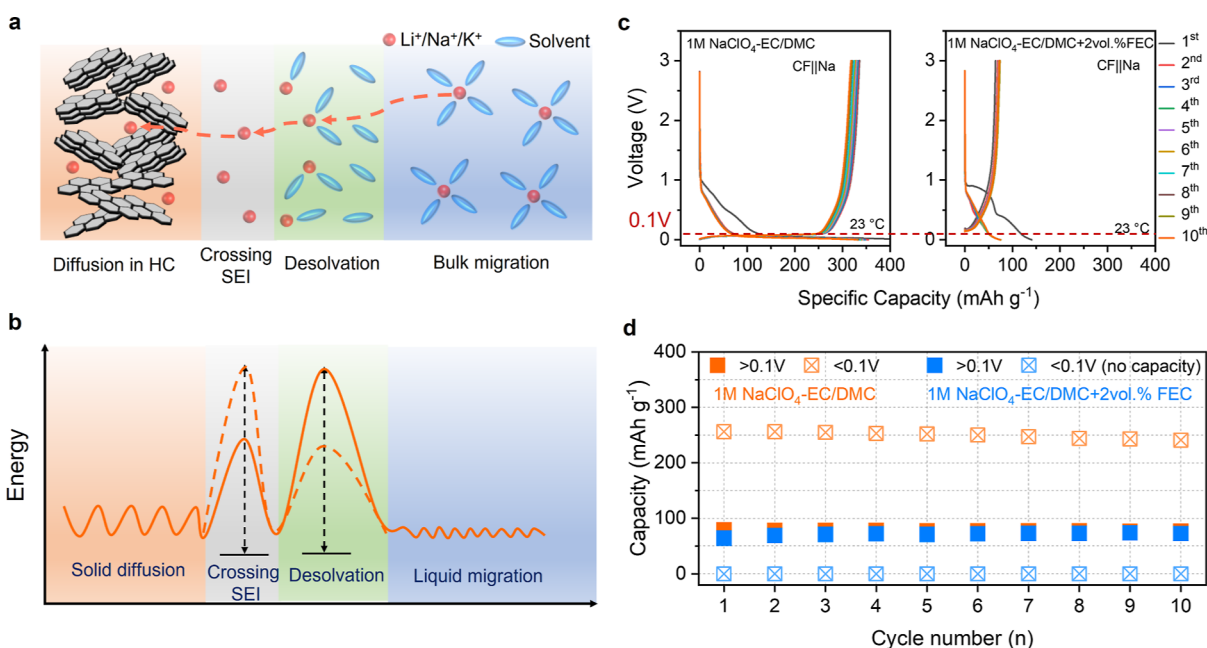


Figure 1. Ion transport in batteries. (a) Working ions (e.g., Li⁺, Na⁺, or K⁺) experience bulk migration, desolvation, SEI crossing, and intercalation into or deposition on the electrode. Hard carbon was used here as an example anode host. (b) The corresponding energy diagram of ion transport. (c) Different Na ion behaviors on hard carbon (CF electrode) in the electrolyte with or without FEC, i.e., voltage profiles show capacities corresponding to adsorption (as characterized by the slope section >0.1 V) and intercalation (as characterized by the plateau section <0.1 V) in the EC/DMC electrolyte, respectively, while only adsorption capacity is observed in the EC/DMC + 2 vol % FEC electrolyte. (d) Corresponding adsorption and intercalation capacities of the CF||Na cell in the EC/DMC and EC/DMC + 2 vol % FEC electrolytes, respectively. Note that the capacity <0.1 V in the presence of FEC is almost zero. The presence of the intercalation capacity shows that Na⁺ has crossed the SEI and intercalated into the CF electrode.

concept of a passive and static layer has also been gradually replaced by that of an active and dynamic entity sensitive to the chemical, electrochemical, and physical environments of the battery cell. Under this new context, an intriguing question arises: Is it possible to achieve switchable ion gating with the SEI?

In this work, we demonstrate that SEIs can be designed to exhibit selective, switchable ion transport properties. When the gate is switched open, working ions transport through SEI to perform intercalation battery chemistry, and when the gate is switched off, the same ions primarily adsorb on the outer surface of the SEI, displaying capacitive behavior. The operation of the open/close gate switch depends on the chemical and structural properties of the few-nanometer-thick inorganic sublayers of the SEI, which are found to be sensitive to temperature, electrolyte additive, electrochemical history, water residue, as well as anode properties. The open/close gate switches can delicately respond to these stimuli with low sensory thresholds, which most likely explains the puzzling, contradictory conclusions about “good” or “bad” SEIs formed under otherwise identical conditions. This mechanistic knowledge about the hitherto unknown ion gating phenomenon will ultimately enable us to precisely tailor desired SEIs as well as heal damaged SEIs in battery environments.

RESULTS AND DISCUSSION

Energy Barriers for Ion Transport in Batteries. Ion transport in a working battery is generally divided into four sequential steps: (i) migration of solvated ions in the bulk electrolyte, (ii) ion desolvation near the electrode surface, (iii) diffusion of naked ions in the SEI layer, and (iv) intercalation or deposition on the electrode (Figure 1a).^{31,32} Each step

requires a distinct activation energy, resulting in ion transport processes with different energy barriers (Figure 1b).^{31,33} The energy barrier to transport solvated ions (step i) in the electrolyte is usually small. Although the energy barrier for the ion transport in the electrode (step iv) is generally higher than that of step (i), it is also very low.^{34,35} Steps (ii) and (iii) at the electrochemical interface involve major energy barriers and are usually rate-determining for battery operation. The solvation structure of the working ion and the chemistry, morphology, and structure of the SEI determine the kinetics of these interfacial processes, which can be tailored by modulating the electrolyte chemistry. We hypothesize that engineered ion gating can reversibly program these two interfacial processes by tailoring their energy barriers. When the working ions transport through the SEI, they can participate in electrode reactions and demonstrate a typical battery process, such as ion intercalation (Figure S1a). However, when the energy barrier becomes too high for ions to transport, they adsorb at the outer surface of the SEI inorganic layer and induce electron accumulation at the inner surface of the SEI inorganic layer, leading to capacitive behavior (Figure S1b). We choose free-standing hard carbon films (CFs) and Na chemistry as the platform to develop these two electrochemical fingerprint signals (i.e., intercalation at <0.1 V and adsorption >0.1 V in Na cells, Figure S2).³⁶ The hard CFs consist of smooth carbon nanofibers (Figure S3) and are used as working electrodes without any additive, allowing for unambiguous SEI characterization. Fluoroethylene carbonate (FEC), one of the most popular electrolyte additives for tailoring SEI properties in alkali ion batteries,^{37–40} triggers a complete shutdown of the Na ion intercalation chemistry at 23 °C, whereas only the adsorption capacity is maintained (Figure 1c,d). Further

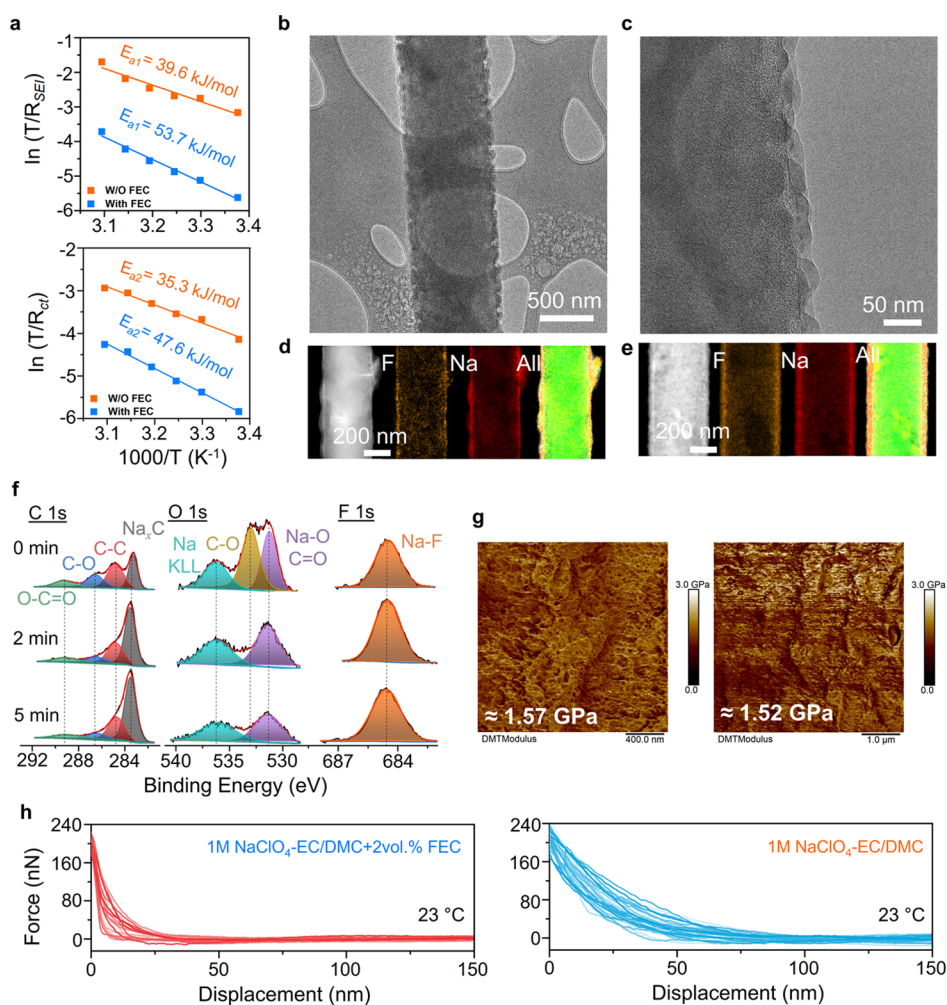


Figure 2. SEI characterization. (a) Arrhenius plots and activation energies of R_{SEI} and R_{ct} derived from temperature-dependent EIS measurements. (b,c) Cryo-TEM images of the CF electrode cycled in the EC/DMC + 2 vol % FEC electrolyte for five cycles. (d,e) STEM–EDS elemental mapping of F, Na, and all elements overlaid in one image (C, O, and Cl elemental maps are shown in Figure S20): (d) cycled at 23 °C and (e) cycled at 60 °C. (f) Depth-profiling XPS spectra of the CF electrode cycled in the EC/DMC + 2 vol % FEC electrolyte for five cycles. (g) AFM modulus images of the CF electrode cycled in the EC/DMC + 2 vol % FEC electrolyte for five cycles. (h) Force–displacement approach curves of the AFM probe toward the SEI formed in the EC/DMC + 2 vol % FEC and EC/DMC electrolyte after one cycle, respectively (showing the inorganic-rich SEI layer in the former electrolyte and organic-rich SEI layer in the latter electrolyte).

control experiments reveal that the CF properties, such as specific surface area, surface functional groups, and defects, can modulate the SEI properties and influence the function of FEC in regulating Na^+ transport through the SEI (Figure S4). Therefore, we adopt the same CF throughout this work to focus on tailoring SEI properties using different electrolytes.

To eliminate the potential impact of Na metal, we evaluated the CF||CF symmetric cell and found that the intercalation capacity also disappears in the electrolyte containing FEC (Figure S5). These results demonstrate that the introduction of FEC as an additive can raise the energy barrier for Na^+ transport in the SEI. We further discovered that the shutdown of Na^+ transport by FEC consistently occurs, even if we change the electrolyte salt and solvent (Figures S6 and S7), chemical vendor (Figure S8), or carbon materials (Figure S9). For example, co-intercalation of Na^+ and solvent molecules takes place in the graphite anode when diglyme is used as the solvent. However, in the presence of FEC (2 vol %), the co-intercalation completely disappeared (Figure S10), further demonstrating that FEC alters the ion transport behavior. The presence of FEC also completely shuts down K^+ intercalation

in the CF (Figure S11a). On the other hand, CFs do not exhibit Li^+ intercalation behavior. The adsorption capacity and cycle life remain nearly identical in Li^+ electrolytes with or without FEC (Figure S11b). Hence, we conclude that FEC in the electrolyte directly modulates the energy barrier for alkali ion transport in the SEI and that we can leverage this electrochemical signature to regulate ion transport through the SEI.

Fluorinated SEI as the Ion Gate. We first estimated the impact of desolvation. Nuclear magnetic resonance (NMR) (Figure S12) and molecular dynamics (MD) simulations (Figure S13) reveal that FEC participates weakly in the solvation structure of Na^+ , while the Na^+ -FEC binding is weaker than the Na^+ -EC and Na^+ -DMC binding (Table S1). Furthermore, the additive level of FEC in the electrolyte is insufficient to populate the solvation sheath of all Na^+ ions; thus, the overall Na^+ -solvent desolvation energy remains essentially unchanged in the presence or absence of 2 vol % FEC. When we modified the solvation structure by increasing the electrolyte concentration to 3 M or decreasing the FEC concentration to 0.5 vol %, we still observed no intercalation

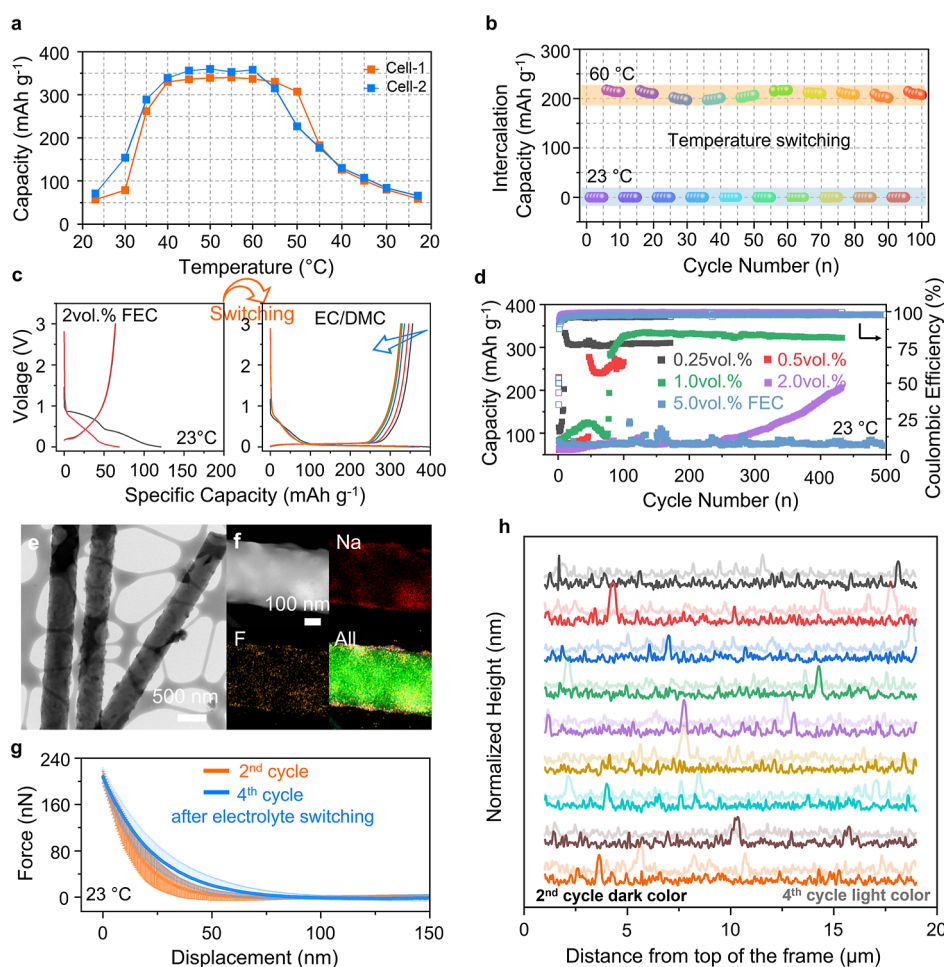


Figure 3. Reversible thermal gating ion transport. (a) Ion transport controlled thermally: the capacity periodically increases and decreases with the round-trip temperature modulation. (b) Open/close gate switching for ion transport: highly reversible capacity with repeated temperature modulations between 23 and 60 °C. (c) Capacity recovery after electrolyte switching, where voltage profiles show the specific capacity before and after electrolyte switching. (d) Long-term cycling performance of the CF||Na cell in the electrolyte with different amounts of FEC additive. (e) Cryo-TEM images of CF electrode after electrolyte switching. (f) STEM-EDS elemental mapping of F, Na, and all elements overlaid in one image. (g) Force–displacement approach curves of AFM probe toward the SEI formed in the 1 M NaClO₄ EC/DMC + 2 vol % FEC electrolyte after two cycles and switching to the 1 M NaClO₄ EC/DMC electrolyte after two cycles, respectively. (h) Corresponding height evolution of the AFM images before and after electrolyte switching.

capacity, confirming that the change in the energy barrier for Na⁺ transport does not exhibit obvious dependence on the Na⁺-solvation structure (Figure S14).

Kinetic analyses were then conducted to evaluate the relative importance of charge transfer and ion diffusion in regulating ion transport. We calculated the energy barriers corresponding to charge transfer and diffusion processes from their temperature-dependent resistances obtained through electrochemical impedance spectra (EIS). The resistances were fitted to Arrhenius equations assuming both processes are thermally activated. The overall impedance in the EC/DMC + 2 vol % FEC electrolyte is consistently much higher than that in the EC/DMC electrolyte at various temperatures, implying a more sluggish Na⁺ kinetics in the former (Figure S15, Tables S2 and S3). The diffusion energy barrier (E_{a1}) in the EC/DMC + 2 vol % FEC electrolyte is higher than that in the EC/DMC electrolyte, showing that the former forms a more resistant SEI (Figure 2a). Furthermore, the activation energy associated with the charge transfer process (E_{a2}) is also much higher in the EC/DMC + 2 vol % FEC electrolyte (Figure 2a). Here, the charge transfer term should include desolvation and inter-

calation. Since the difference in desolvation energy is negligible between these two electrolytes, Na⁺ intercalation in the FEC-containing electrolyte requires higher activation energy. These results suggest that the SEI chemistry governs whether the Na⁺ intercalation can occur.

We then turned our attention to the uniqueness of FEC-derived SEI. Based on cyclic voltammetry (CV), we found that FEC starts to undergo reductive decomposition at ≈ 1.0 V, far higher than the reductive decomposition of EC/DMC (Figure S16). DFT calculations reveal that FEC has a lower LUMO level because the strongly electron-withdrawing fluorine polarizes the FEC molecule in contrast to the non-fluorinated counterpart EC, leading to preferential reductive decomposition of FEC at higher potentials to form SEI (Table S1). Furthermore, FEC can drastically transform the morphology and composition of SEI. We observed a thick, heterogeneous, and rough SEI formed on CFs recovered from the baseline EC/DMC electrolyte (Figure S17a). Cryo-TEM characterization further shows that this SEI is mostly amorphous and randomly covers the fiber surface (Figure S18). XPS results show that the amorphous SEI is enriched with organic

compounds resulting from the solvent (EC/DMC) reduction (Figure S19 and Table S4). In contrast, the FEC-containing electrolyte results in a smooth, compact, and uniform SEI layer (Figure S17b). Cryo-TEM and fast Fourier transform (FFT) analyses show that the CF surface is fully covered by an SEI layer that is enriched with NaF nanodomains (Figures 2b,c and S20). EDS mapping shows that the CF surface is densely populated with Na and F (Figure 2d), which becomes more uniform after cycling at 60 °C (Figure 2e). Furthermore, XPS results show that the SEI formed in the FEC-containing electrolyte has much lower organic contents and a higher NaF concentration in its inner layer (Figures 2f, S21, and Table S5).

The mechanical properties of the formed SEI layer are probed by AFM. The SEI formed in the EC/DMC electrolyte consists of two regions with different moduli. The softer SEI area has a modulus of 0.98 GPa, and the harder area is about 1.20 GPa, suggesting uneven SEI layer distribution (Figure S22). The SEI formed in the EC/DMC + 2 vol % FEC electrolyte appears uniform and shows a much more consistent modulus around 1.52–1.57 GPa (Figure 2g). The higher modulus implies a higher density of inorganic species. We then produced SEIs in situ on a disordered carbon electrode⁴¹ (Figure S23a,b), which has a smooth surface and allows for more incisive mechanical measurements at many equivalent regions on the electrode. The AFM tip experiences increasing force as it pushes on the SEI formed on the electrode surface (Figures 2h and S23c,d). In the EC/DMC + 2 vol % FEC electrolyte, the force starts to increase at a 25 nm displacement from the electrode surface. After switching the in situ cell to the EC/DMC electrolyte, the SEI is reformed, and the force starts to increase at a 75 nm distance, indicating a much thicker and softer SEI formed by the EC/DMC electrolyte. In addition, the slope of the force increase is much larger in the EC/DMC + 2 vol % FEC electrolyte, further supporting that the SEI is enriched with dense inorganic compounds (e.g., NaF).

Nudged elastic band (NEB) calculations conducted by Li et al. demonstrate that Na⁺ diffusion across the NaF-rich SEI layer requires more energy.⁴² This theory explains our observation of suppressed Na⁺ intercalation. Furthermore, the intercalation capacity reappears when 0.2 vol % water is added to the EC/DMC + 2 vol % FEC electrolyte (Figure S24), because NaF is soluble in water, leading to NaF layer defects. These results strongly suggest that NaF is the main species responsible for blocking Na⁺ transport.

Open/Close Gate Switching for Ion Transport. Since ion diffusion through SEI is a kinetically driven process, we conjectured that temperature can be exploited to control the diffusion properties. Meanwhile, modulating temperature can also alter the composition, morphology, and structure of the SEI, which can in turn alter the ion–SEI interaction and consequently the electrochemical behaviors, i.e., intercalation versus adsorption. We identified the sensitivity of the gate switch to temperature and investigated the switching reversibility. Consistent with Figure 1c, the energy barrier is too high for Na⁺ diffusion through the SEI at 23 °C. The capacity starts to increase at 30 °C and reaches a capacity of 300 mA h g⁻¹ at 35 °C (Figure 3a), which is similar to the full capacity achieved in the EC/DMC electrolyte (Figure 1c). The increased capacity comes from the plateau region of the voltage profile, contributed by the recovery of the Na⁺ intercalation chemistry at even slightly elevated temperatures (Figure S25). It should be noted that most studies have reported battery

performance within the 23–35 °C temperature window, which is often designated as “room temperature” in the literature. Our results show that the capacity changes drastically within such a narrow temperature window due to the impact of various SEI chemistries on ion transport, which explains the seemingly conflicting conclusions drawn by different studies with regard to the same electrolyte additive. As the temperature decreases, the plateau capacity gradually decays and disappears completely after returning to 23 °C. Such a reversible switching function also applies to a rich range of other Na electrolytes containing FEC (Figure S26). By applying repeated temperature swings between 23 and 60 °C, we demonstrate the robust reversibility of the open/close gate switching (Figures 3b and S27), where the intercalation capacity appears and disappears under the two thermal conditions. This phenomenon also applies to the CF||K cells, where high temperature opens the gate and allows K⁺ transport, while lower temperature closes the gate and blocks K⁺ transport (Figure S28).

Open/Close Gate Switching Governed by SEI Dissolution/Regrowth Dynamics. Besides the thermal activation of ion transport following the Arrhenius relationship, the dynamic evolution of the SEI at different temperatures also plays a critical role in operating the ion gating function. There is a dynamic NaF dissolution and SEI-regrowth process during electrochemical cycling, which offers an additional mechanism for ion gating. The dissolution–regrowth equilibrium is also influenced by the precursor of the NaF-based SEI, i.e., FEC in the present case. The regrowth of a dense NaF layer at 23 °C is key to closing the gate. We pre-formed a NaF layer on CFs in the EC/DMC + 2 vol % FEC electrolyte and then transplanted the cycled CFs to FEC-free electrolyte at 23 °C, only to find that the intercalation capacity quickly recovers within a few cycles (Figure 3c), indicating a rapid loss of ion gating function when there is no FEC in the bulk electrolyte. When we used other baseline electrolytes, we observed the same phenomenon after FEC was removed from the electrolytes (Figure S29).

Since SEI dissolution can take place throughout the entire battery life during electrochemical cycling or storage, the sustainable supply of FEC becomes critical for NaF regrowth and, thus, for gate closing. Figures 3d and S30 show the cycling performance of CFs in the EC/DMC electrolyte with different initial FEC concentrations. With 0.25 and 0.5 vol % FEC, the intercalation capacity recovers within 50 cycles. With an increase to 1 vol % FEC, the intercalation capacity is able to be recovered after 100 cycles. With a continuing increase to 2 vol % FEC or 5 vol % FEC, more cycles are required for intercalation capacity recovery.

In the EC/DMC + 2 vol % FEC electrolyte, SEM images reveal that a dense SEI layer uniformly covered the CFs even after cycling at 60 °C (Figure S31), consistent with the STEM-EDS mapping and HRTEM images, where the F and Na signals become stronger and a thicker SEI layer with distinct lattice fringes covers the CFs (Figures 2e and S32). After switching to the EC/DMC electrolyte, the SEI morphology becomes rough, with concomitant loss of NaF crystalline domains in the SEI, due to the dissolution of the NaF-rich SEI and the growth of a new SEI (Figures 3e,f and S33–S35). AFM force–displacement curves also demonstrate the SEI dissolution and regrowth after the electrolyte switching, where the force representing the dense SEI layer gradually becomes dispersed, indicating a progressively rough and non-uniform SEI (Figure 3g). The dynamic changes of AFM height profiles

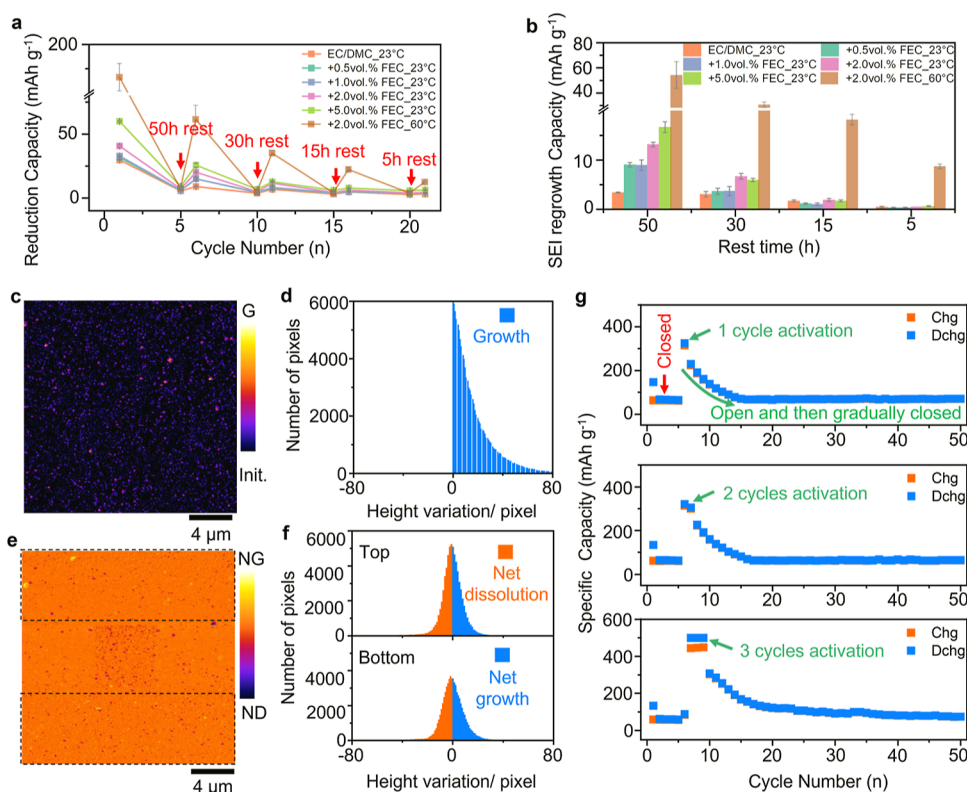


Figure 4. SEI dissolution and regrowth. (a) Reduction (discharge) capacity comes from the reduction reaction between the Cu and electrolyte, corresponding to the formation of SEI. The evolution of the reduction capacity implies that SEI undergoes changes in dissolution and regrowth dynamics. After each rest, the reduction capacity picks up again but is lower than the initial reduction capacity, implying that the SEI undergoes partial dissolution during each rest. (b) SEI regrowth capacity after different rest durations. (c) Height variation images from AFM analysis by subtracting the pristine disordered carbon electrode from the first cycled electrode (in the 1 M NaClO₄/EC/DMC + 2 vol % FEC electrolyte, G here is growth, and Init. is initial). (d) The corresponding height variation distribution shows the SEI growth after the first cycle. (e) Height variation images from AFM analysis by subtracting the first cycled electrode from the second cycled electrode (in the 1 M NaClO₄/EC/DMC + 2 vol % FEC electrolyte, NG here is net growth, and ND is net dissolution). (f) The corresponding height variation distribution shows the heterogeneous SEI dissolution (net dissolution) and regrowth (net growth) after the second cycle. (g) The activation process (low-voltage activation) promotes capacity recovery, but then the capacity gradually decreases as the SEI regrowth blocks ion transport again.

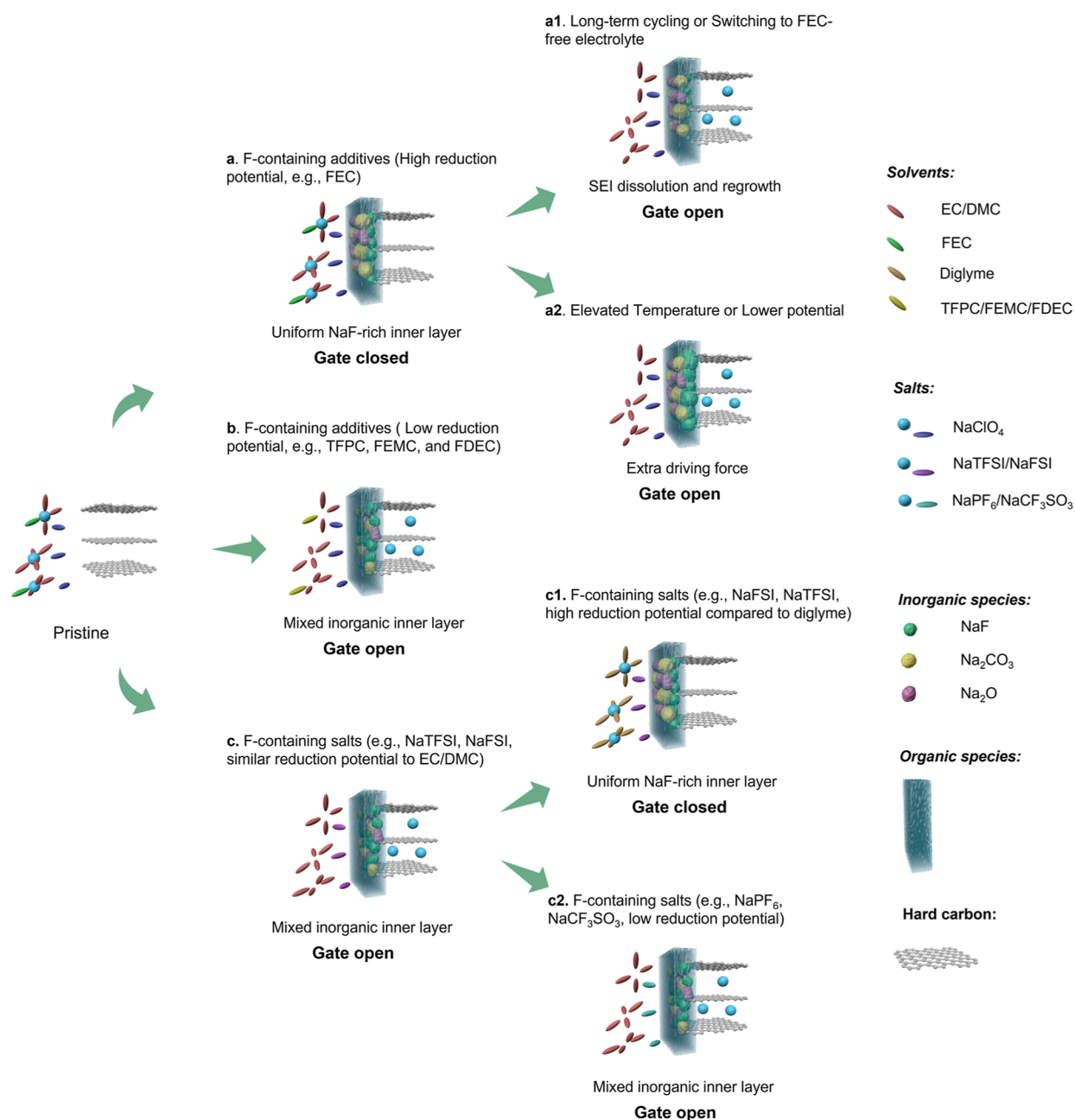
before and after electrolyte switching can show the SEI dissolution and regrowth (Figures 3h and S36).

To further prove that the SEI dissolution and regrowth is a dynamic process, we now directly grow SEI on a Cu surface.⁴³ The Cu/Na cell is cycled in the 0.002–2 V range, which ensures no Na metal plating. Thus, the irreversible reduction (discharge) capacity solely originates from the SEI formation, and its evolution should directly reflect the SEI formation, dissolution, and regrowth. Resting the cell at the 2 V state for x h ($x = 50, 30, 15,$ and 5 h) after every five cycles allows the SEI to dissolve and then polarizing the cell negatively again in the same voltage window enables SEI regrowth (Figure S37). Figure 4a shows the first reduction capacity associated with the initial SEI formation and the following reduction capacities at the 6th, 11th, 16th, and 21st cycles after an open circuit rest for 50, 30, 15, and 5 h, respectively. The FEC-containing electrolyte shows a higher initial SEI formation capacity due to the FEC decomposition, and such a trend persisted during the first 15 cycles. After that, the SEI dissolution becomes negligible at 23 °C, indicating that the SEI stabilizes and reaches a dissolution and regrowth equilibrium. SEI dissolution is more evident during the rest in the FEC-containing electrolyte and the elevated temperature accelerates the SEI dissolution. Figure 4b shows the capacity associated with the SEI regrowth after each x h-long rest, where we find that the

SEI regrowth capacity is higher in the FEC-containing electrolyte, indicating that SEI dissolution and regrowth are more severe in the FEC-containing electrolyte and providing a mechanism for the intercalation capacity recovery after long-term cycling (Figure 3c). Moreover, the electrolyte decomposition is accelerated at 60 °C, resulting in much higher SEI regrowth capacities. Note here that the measurement is conducted on a planar Cu electrode with a low surface area. The SEI dissolution and regrowth on the CF electrode should be more drastic due to its higher surface area.

The AFM results further confirm the SEI dissolution and regrowth in the FEC-containing electrolyte. The disordered carbon electrode shows a smooth surface (Figure S38a).⁴¹ After the first cycle, the surface becomes rough, and the SEI formation is clearly visible (Figures 4c and S38b). The height variation per pixel only sees an increasing trend, further indicating an SEI growth (Figure 4d). Subsequently (second cycle), we observed the SEI layer undergoing simultaneous dissolution (net dissolution) and regrowth (net growth) in different regions, as determined by the changing height profiles (Figures 4e, and S38c). The height represents the roughness of the SEI, where the evolution of the height distribution shows the SEI dissolution and regrowth after the second cycle (Figure 4f).

Scheme 1. Summary of the SEI Properties Responses for Ion Transport in Na Ion Batteries: (a) For FEC Additives, the High Reduction Potential (~ 1.0 V) of FEC Enables It to be Preferentially Decomposed over EC/DMC, Forming a NaF-Rich Uniform SEI Layer and Covering the Intercalation Sites: the High Energy Barrier of NaF Hinders Na Ions from Transporting through These Intercalation Sites, Thus Closing the Gate and Suppressing Intercalation Capacity: However, the NaF is Not Stable and Can Gradually Dissolve in the Electrolyte: (a1) after Switching to FEC-Free Electrolyte, NaF Gradually Dissolves and Cannot be Replenished, Na Ions Can Transport through the Intercalation Sites, and the Intercalation Capacity Recovers: For Long-Term Cycling, NaF Undergoes Simultaneous Dissolution and Regrowth: When FEC is Fully Consumed and Insufficient to Replenish Exposed Intercalation Sites, the Intercalation Capacity Recovers: (a2) Elevated Temperature or Lower Potential Can Provide Drive Forces to Overcome the Energy Barrier to Allow for Na Ion Transport through the Intercalation Sites, and Thus the Intercalation Capacity Recovers: (b,c) For Other F-Containing Additives and Na Salts, the Reduction Potential Determines Ion Transport: When the Reduction Potential of Additives and Na Salts is Similar to the EC/DMC Solvent, the Intercalation Sites are Covered by Mixed Inorganic Species ($\text{Na}_2\text{O}/\text{NaF}/\text{Na}_2\text{CO}_3$), and Na Ions Can be Transported through These Low-Energy Barrier Sites to Achieve Intercalation Capacity: (c1) after Switching to a Stable Diglyme Solvent, the NaTFSI and NaFSI Decompose Preferentially, and the Intercalation Sites are Mostly Covered by NaF, Which Blocks Ion Transport and Provides No Intercalation Capacity: (c2) When the Na Salts also Contain Other Elements besides F Such as S, C, and P (NaCF_3SO_3 , NaPF_6), the Intercalation Sites Are Covered by Mixed Inorganic Species, and Na Ions Can Transport through These Low-Energy Barrier Sites to Achieve Intercalation Capacity



Healing Ion Gating after Damage. Ion gating through dissolution/regrowth dynamics has also shown strong resilience against interruption and can be healed even after it is damaged. We first cycle the CF||Na cell cycled in the FEC-containing electrolyte for five cycles to form a stable SEI. Consistent with our earlier finding, there is no intercalation capacity due to the closed ion gate (Figure 4g). Then, we decrease the discharge lower cutoff voltage to -50 mV for one and two cycles (i.e., low-voltage activation). Note that Na plating does not occur at this voltage (Figure S39a,b). We observe that the intercalation capacity is recovered to above 300 mA h g^{-1} (Figures 4g, and S39a,b), which is the consequence that the ion gating can be switched open by providing an extra driving force in the form of discharge overpotential. After increasing the lower cutoff voltage to 0 V, we gradually close the ion gating, and the intercalation capacity gradually decreases to its original level (same as the first five cycles). Even if we perform Na plating and stripping for three cycles to damage the ion gating (Figure S39c), the ion gating can still be gradually restored to the closed state after increasing the lower cutoff voltage to 0 V (Figure 4g, bottom), showing that the residual FEC is decomposed again to compensate for the SEI dissolution.

Roles of Reduction Potentials in Creating the NaF Ion Gating: F-Containing Salts and Additives. FEC has a much higher reduction potential than EC and DMC because fluorination makes it the main SEI contributor before EC and DMC can be reduced. In addition, the NaF nucleation at a high potential also allows NaF to continuously grow during the discharge and form a dense layer of large-grain NaF ideal for ion gating. We conjecture that the reduction potentials of the F-containing electrolyte components might be as important as the chemical composition of the SEI in determining the functioning of the NaF ion gating. To prove such a hypothesis, 3,3,3-trifluoropropylene carbonate (TFPC), bis-(2,2,2-trifluoroethyl) carbonate (FDEC), and methyl (2,2,2-trifluoroethyl) carbonate (FEMC) are used as F-containing additives. These additives also weakly interact with Na^+ (Figure S13g,h). The decomposition potentials of these additives are all around 0.5 V (Figure S40), similar to those of EC and DMC. Consequently, none of these additives were able to form Na^+ blocking SEIs (Figure S41), despite the fact that the SEI formed in the presence of these additives is four times more highly fluorinated than that formed by the FEC-containing electrolyte (Figure S42 and Table S6). This result strongly implies that an inorganic SEI inner layer with mixed ingredients contributed by the decomposition products of oxides or carbonates cannot block the ion transport.

We further verify this conclusion by using electrolytes with different F-containing anions including NaTFSI, NaFSI, and $NaCF_3SO_3$ in both ester (EC, DMC) and ether (diglyme) solvents. Diglyme is a stable solvent that does not undergo reductive decomposition, while NaTFSI, NaFSI, and $NaCF_3SO_3$ all have decomposition potentials around 0.5 V vs Na/Na^+ , but the distributions of decomposition products are different. In the 1 M NaTFSI diglyme electrolyte, no intercalation capacity is observed (Figure S43a). After switching to the 1 M NaTFSI EC/DMC electrolyte, the intercalation capacity is mostly recovered (Figure S43b). Electrochemical decomposition of NaFSI can lead to more diverse Na compounds than that of NaTFSI; thus, we observed a slightly higher intercalation capacity in the 1 M NaFSI diglyme electrolyte due to the weakened ion gating function

(Figure S43c). Similarly, after switching to the 1 M NaFSI EC/DMC electrolyte, the intercalation capacity is mostly recovered (Figure S43d). The ion gating function is further weakened in the 1 M $NaCF_3SO_3$ diglyme electrolyte, due to the fact that the $NaCF_3SO_3$ decomposition leads to more diverse reduction products (Figure S43e).

We summarize our discoveries in Scheme 1. During the first discharge, FEC begins to decompose to form NaF at a high potential before the decomposition of other electrolyte components. Thus, NaF starts to grow and gradually forms a dense layer on the CF surface to block the Na ion transport through SEI. Elevated temperatures and large discharge overpotentials both serve as driving forces to overcome the energy barrier to enable Na ion transport through SEI. At lower temperatures, the ion gate is closed. Upon switching to FEC-free electrolytes, NaF experienced dissolution, leading to Na ion transport through SEI and recovery of intercalation capacity. The reversible operation of the ion gating is also governed by the SEI dissolution/regrowth dynamics. Upon long-term cycling, once the SEI regrowth kinetics cannot outmatch the SEI dissolution kinetics, the ion gating is switched open. The formation of a dense NaF layer, with low contents of other Na compounds, is critical for creating the ion gating effect. Thus, the electrolyte chemistry that produces mixed inorganic Na compounds fails to form a strong ion-gating effect.

CONCLUSIONS

We have found a hitherto unknown aspect of SEI that serves as a thermally activated transport gating, which can switch the electrochemical behaviors of the working ions between intercalation batteries (gate open) and double-layer capacitor (gate close). The dynamic evolution of the NaF-enriched SEI layer during thermal switching is key to achieving such an ion-gating design. Furthermore, elevated temperature also provides thermal energy to overcome the ion transport energy barrier. The reduction potentials of fluorinated additives and F-containing salts govern the chemistry and structure of the inorganic inner-layer of the SEI, which dictates the formation and function of the ion gating. The dissolution and regrowth dynamics of NaF under operating conditions determine the operability and reversibility of the ion gating switch. The ion gating exhibits strong resilience against interruption and can be healed even after damage. This previously unknown function of SEI and its high sensitivity to different stimuli explain why researchers reported completely opposite conclusions regarding whether a certain electrolyte additive is a good or a bad SEI-forming agent. These critical insights will guide us in designing better interphases for future battery chemistries.

ASSOCIATED CONTENT

Data Availability Statement

All relevant data in the article are available from the corresponding author upon reasonable request.

Supporting Information

The Supporting Information is available free of charge at <https://pubs.acs.org/doi/10.1021/jacs.3c03429>.

Materials and methods, electrochemical measurements, SEM and TEM images, molecular dynamics simulation, XPS spectra and quantification, and AFM images (PDF)

AUTHOR INFORMATION

Corresponding Authors

Hui Xiong – Micron School of Materials Science and Engineering, Boise State University, Boise, Idaho 83725, United States; Center for Advanced Energy Studies, Idaho Falls, Idaho 83401, United States; orcid.org/0000-0003-3126-1476; Email: clairexiong@boisestate.edu

Peng Bai – Department of Energy, Environment & Chemical Engineering, Washington University in St. Louis, St. Louis, Missouri 63130, United States; orcid.org/0000-0002-2419-3498; Email: pbai@wustl.edu

Kang Xu – Battery Science Branch, US Army Research Laboratory, Adelphi, Maryland 20783, United States; Email: conrad.k.xu.civ@mail.mil

Feng Lin – Department of Chemistry, Virginia Tech, Blacksburg, Virginia 24061, United States; Macromolecules Innovation Institute, Virginia Tech, Blacksburg, Virginia 24061, United States; orcid.org/0000-0002-3729-3148; Email: fenglin@vt.edu

Authors

Lei Tao – Department of Chemistry, Virginia Tech, Blacksburg, Virginia 24061, United States

Joshua A. Russell – Micron School of Materials Science and Engineering, Boise State University, Boise, Idaho 83725, United States

Dawei Xia – Department of Chemistry, Virginia Tech, Blacksburg, Virginia 24061, United States; orcid.org/0000-0003-4265-2528

Bingyuan Ma – Department of Energy, Environment & Chemical Engineering, Washington University in St. Louis, St. Louis, Missouri 63130, United States

Sooyeon Hwang – Center for Functional Nanomaterials, Brookhaven National Laboratory, Upton, New York 11973, United States; orcid.org/0000-0001-5606-6728

Zhijie Yang – Department of Chemistry, Virginia Tech, Blacksburg, Virginia 24061, United States

Anyang Hu – Department of Chemistry, Virginia Tech, Blacksburg, Virginia 24061, United States; orcid.org/0000-0003-0669-9126

Yuxin Zhang – Department of Chemistry, Virginia Tech, Blacksburg, Virginia 24061, United States; orcid.org/0000-0002-2830-4159

Poom Sittisomwong – Department of Energy, Environment & Chemical Engineering, Washington University in St. Louis, St. Louis, Missouri 63130, United States

Deyang Yu – Department of Chemistry, Virginia Tech, Blacksburg, Virginia 24061, United States; orcid.org/0000-0003-0587-1211

Paul A. Deck – Department of Chemistry, Virginia Tech, Blacksburg, Virginia 24061, United States; Macromolecules Innovation Institute, Virginia Tech, Blacksburg, Virginia 24061, United States; orcid.org/0000-0002-1069-1496

Louis A. Madsen – Department of Chemistry, Virginia Tech, Blacksburg, Virginia 24061, United States; Macromolecules Innovation Institute, Virginia Tech, Blacksburg, Virginia 24061, United States; orcid.org/0000-0003-4588-5183

Haibo Huang – Department of Food Science and Technology, Virginia Tech, Blacksburg, Virginia 24061, United States; orcid.org/0000-0002-2106-4105

Complete contact information is available at:
<https://pubs.acs.org/10.1021/jacs.3c03429>

Author Contributions

[○]J.R., D.X., B.M., and S.H. contributed equally to the work.

Notes

The authors declare no competing financial interest.

ACKNOWLEDGMENTS

The work is primarily supported by the USDA AFRI Foundational and Applied Program (grant number 2020-67021-31139), the Institute for Critical Technology and Applied Science, and the Lay Nam Chang Dean's Discovery Fund at Virginia Tech. H.H. acknowledges support from the Virginia Agriculture Experiment Station and the Hatch Program of the National Institute of Food and Agriculture (NIFA), USDA. This work used shared facilities at the Virginia Tech National Center for Earth and Environmental Nanotechnology Infrastructure (NanoEarth), a member of the National Nanotechnology Coordinated Infrastructure (NNCI), supported by NSF (ECCS 1542100 and ECCS 2025151). This work was partly supported by the National Science Foundation grant (award no. 1934122). The material characterization experiments were partly supported by the Institute of Materials Science and Engineering (IMSE) at Washington University in Saint Louis (WUSTL). P.B. acknowledges the faculty start-up support from WUSTL and a gift fund from TSVC. P.S. acknowledges the fellowship support from the McDonnell International Scholars Academy at WUSTL. J.R. and H.X. acknowledge the support by the U.S. Department of Energy, Office of Science, Office of Basic Energy Sciences program under award number DE-SC0019121 and the Graduate Assistantship from Micron School of Materials Science and Engineering, College of Engineering, at Boise State. The use of the environmental AFM was supported by NSF MRI (grant no. 1727026). This research used electron microscopy resources of the Center for Functional Nanomaterials (CFN), which is a U.S. Department of Energy Office of Science User Facility, at Brookhaven National Laboratory under contract no. DE-SC0012704. J.R. and H.X. thank J. May and I. F. Cheng from the University of Idaho for supplying the disordered carbon samples for AFM measurements.

REFERENCES

- (1) Lu, L.; Han, X.; Li, J.; Hua, J.; Ouyang, M. A Review on the Key Issues for Lithium-Ion Battery Management in Electric Vehicles. *J. Power Sources* **2013**, *226*, 272–288.
- (2) Bandhauer, T. M.; Garimella, S.; Fuller, T. F. A Critical Review of Thermal Issues in Lithium-Ion Batteries. *J. Electrochem. Soc.* **2011**, *158*, R1.
- (3) Tarascon, J. M.; Armand, M. Issues and Challenges Facing Rechargeable Lithium Batteries. *Nature* **2001**, *414*, 359–367.
- (4) Fong, R.; von Sacken, U.; Dahn, J. R. Studies of Lithium Intercalation into Carbons Using Nonaqueous Electrochemical Cells. *J. Electrochem. Soc.* **1990**, *137*, 2009–2013.
- (5) Heiskanen, S. K.; Kim, J.; Lucht, B. L. Generation and Evolution of the Solid Electrolyte Interphase of Lithium-Ion Batteries. *Joule* **2019**, *3*, 2322–2333.
- (6) Winter, M. The Solid Electrolyte Interphase - The Most Important and the Least Understood Solid Electrolyte in Rechargeable Li Batteries. *Z. Phys. Chem.* **2009**, *223*, 1395–1406.
- (7) Verma, P.; Maire, P.; Novák, P. A Review of the Features and Analyses of the Solid Electrolyte Interphase in Li-Ion Batteries. *Electrochim. Acta* **2010**, *55*, 6332–6341.
- (8) Goodenough, J. B.; Park, K. S. The Li-Ion Rechargeable Battery: A Perspective. *J. Am. Chem. Soc.* **2013**, *135*, 1167–1176.

- (9) Aurbach, D.; Markovsky, B.; Levi, M. D.; Levi, E.; Schechter, A.; Moshkovich, M.; Cohen, Y. New Insights into the Interactions between Electrode Materials and Electrolyte Solutions for Advanced Nonaqueous Batteries. *J. Power Sources* **1999**, *81*–82, 95–111.
- (10) Peled, E.; Golodnitsky, D.; Ardel, G. Advanced Model for Solid Electrolyte Interphase Electrodes in Liquid and Polymer Electrolytes. *J. Electrochem. Soc.* **1997**, *144*, L208–L210.
- (11) Peled, E. The Electrochemical Behavior of Alkali and Alkaline Earth Metals in Nonaqueous Battery Systems—The Solid Electrolyte Interphase Model. *J. Electrochem. Soc.* **1979**, *126*, 2047–2051.
- (12) Dey, A. N.; Sullivan, B. P. The Electrochemical Decomposition of Propylene Carbonate on Graphite. *J. Electrochem. Soc.* **1970**, *117*, 222.
- (13) Xu, K. Li-Ion Battery Electrolytes. *Nat. Energy* **2021**, *6*, 763.
- (14) Swallow, J. E. N.; Fraser, M. W.; Kneusels, N.-J. H.; Charlton, J. F.; Sole, C. G.; Phelan, C. M. E.; Björklund, E.; Bencok, P.; Escudero, C.; Pérez-Dieste, V.; Grey, C. P.; Nicholls, R. J.; Weatherup, R. S. Revealing Solid Electrolyte Interphase Formation through Interface-Sensitive Operando X-Ray Absorption Spectroscopy. *Nat. Commun.* **2022**, *13*, 6070.
- (15) Gao, Y.; Yan, Z.; Gray, J. L.; He, X.; Wang, D.; Chen, T.; Huang, Q.; Li, Y. C.; Wang, H.; Kim, S. H.; Mallouk, T. E.; Wang, D. Polymer–Inorganic Solid–Electrolyte Interphase for Stable Lithium Metal Batteries under Lean Electrolyte Conditions. *Nat. Mater.* **2019**, *18*, 384–389.
- (16) Hope, M. A.; Rinkel, B. L. D.; Gunnarsdóttir, A. B.; Märker, K.; Menkin, S.; Paul, S.; Sergeev, I. v.; Grey, C. P. Selective NMR Observation of the SEI–Metal Interface by Dynamic Nuclear Polarisation from Lithium Metal. *Nat. Commun.* **2020**, *11*, 2224.
- (17) Zhang, Z.; Li, Y.; Xu, R.; Zhou, W.; Li, Y.; Oyakhire, S. T.; Wu, Y.; Xu, J.; Wang, H.; Yu, Z.; Boyle, D. T.; Huang, W.; Ye, Y.; Chen, H.; Wan, J.; Bao, Z.; Chiu, W.; Cui, Y. Capturing the Swelling of Solid-Electrolyte Interphase in Lithium Metal Batteries. *Science* **2022**, *375*, 66–70.
- (18) Wang, L.; Menakath, A.; Han, F.; Wang, Y.; Zavalij, P. Y.; Gaskell, K. J.; Borodin, O.; Iuga, D.; Brown, S. P.; Wang, C.; Xu, K.; Eichhorn, B. W. Identifying the Components of the Solid–Electrolyte Interphase in Li-Ion Batteries. *Nat. Chem.* **2019**, *11*, 789–796.
- (19) Fang, C.; Li, J.; Zhang, M.; Zhang, Y.; Yang, F.; Lee, J. Z.; Lee, M. H.; Alvarado, J.; Schroeder, M. A.; Yang, Y.; Lu, B.; Williams, N.; Ceja, M.; Yang, L.; Cai, M.; Gu, J.; Xu, K.; Wang, X.; Meng, Y. S. Quantifying Inactive Lithium in Lithium Metal Batteries. *Nature* **2019**, *572*, 511–515.
- (20) Shadike, Z.; Lee, H.; Borodin, O.; Cao, X.; Fan, X.; Wang, X.; Lin, R.; Bak, S. M.; Ghose, S.; Xu, K.; Wang, C.; Liu, J.; Xiao, J.; Yang, X. Q.; Hu, E. Identification of LiH and Nanocrystalline LiF in the Solid–Electrolyte Interphase of Lithium Metal Anodes. *Nat. Nanotechnol.* **2021**, *16*, 549–554.
- (21) Edström, K.; Herstedt, M.; Abraham, D. P. A New Look at the Solid Electrolyte Interphase on Graphite Anodes in Li-Ion Batteries. *J. Power Sources* **2006**, *153*, 380–384.
- (22) Zhang, Q.; Pan, J.; Verbrugge, M. W.; Lu, P.; Liu, Z.; Sheldon, B. W.; Cheng, Y. T.; Qi, Y.; Xiao, X. Synergetic Effects of Inorganic Components in Solid Electrolyte Interphase on High Cycle Efficiency of Lithium Ion Batteries. *Nano Lett.* **2016**, *16*, 192–2016.
- (23) Liu, T.; Lin, L.; Bi, X.; Tian, L.; Yang, K.; Liu, J.; Li, M.; Chen, Z.; Lu, J.; Amine, K.; Xu, K.; Pan, F. In Situ Quantification of Interphasial Chemistry in Li-Ion Battery. *Nat. Nanotechnol.* **2018**, *14*, 50–56.
- (24) Cresce, A. V.; Russell, S. M.; Baker, D. R.; Gaskell, K. J.; Xu, K. In Situ and Quantitative Characterization of Solid Electrolyte Interphases. *Nano Lett.* **2014**, *14*, 1405–1412.
- (25) Tikekar, M. D.; Choudhury, S.; Tu, Z.; Archer, L. A. Design Principles for Electrolytes and Interfaces for Stable Lithium-Metal Batteries. *Nat. Energy* **2016**, *1*, 16114–16117.
- (26) Li, Y.; Leung, K.; Qi, Y. Computational Exploration of the Li-Electrode/Electrolyte Interface in the Presence of a Nanometer Thick Solid-Electrolyte Interphase Layer. *Acc. Chem. Res.* **2016**, *49*, 2363–2370.
- (27) Zhou, Y.; Su, M.; Yu, X.; Zhang, Y.; Wang, J. G.; Ren, X.; Cao, R.; Xu, W.; Baer, D. R.; Du, Y.; Borodin, O.; Wang, Y.; Wang, X. L.; Xu, K.; Xu, Z.; Wang, C.; Zhu, Z. Real-Time Mass Spectrometric Characterization of the Solid–Electrolyte Interphase of a Lithium-Ion Battery. *Nat. Nanotechnol.* **2020**, *15*, 224–230.
- (28) Lu, J.; Wu, T.; Amine, K. State-of-the-Art Characterization Techniques for Advanced Lithium-Ion Batteries. *Nat. Energy* **2017**, *2*, 17011–17013.
- (29) Xu, K. Electrolytes and Interphases in Li-Ion Batteries and Beyond. *Chem. Rev.* **2014**, *114*, 11503–11618.
- (30) Wang, C.; Meng, Y. S.; Xu, K. Perspective—Fluorinating Interphases. *J. Electrochem. Soc.* **2018**, *166*, A5184–A5186.
- (31) Persson, K.; Sethuraman, V. A.; Hardwick, L. J.; Hinuma, Y.; Meng, Y. S.; van der Ven, A.; Srinivasan, V.; Kostecki, R.; Ceder, G. Lithium Diffusion in Graphitic Carbon. *J. Phys. Chem. Lett.* **2010**, *1*, 1176–1180.
- (32) Cao, W.; Li, Q.; Yu, X.; Li, H. Controlling Li Deposition below the Interface. *eScience* **2022**, *2*, 47–78.
- (33) Shi, S.; Lu, P.; Liu, Z.; Qi, Y.; Hector, L. G.; Li, H.; Harris, S. J. Direct Calculation of Li-Ion Transport in the Solid Electrolyte Interphase. *J. Am. Chem. Soc.* **2012**, *134*, 15476–15487.
- (34) Xu, K.; Lam, Y.; Zhang, S. S.; Jow, T. R.; Curtis, T. B. Solvation Sheath of Li⁺ in Nonaqueous Electrolytes and Its Implication of Graphite/ Electrolyte Interface Chemistry. *J. Phys. Chem. C* **2007**, *111*, 7411–7421.
- (35) Qi, Y.; Guo, H.; Hector, L. G.; Timmons, A. Threefold Increase in the Young's Modulus of Graphite Negative Electrode during Lithium Intercalation. *J. Electrochem. Soc.* **2010**, *157*, A558.
- (36) Qiu, S.; Xiao, L.; Sushko, M. L.; Han, K. S.; Shao, Y.; Yan, M.; Liang, X.; Mai, L.; Feng, J.; Cao, Y.; Ai, X.; Yang, H.; Liu, J. Manipulating Adsorption–Insertion Mechanisms in Nanostructured Carbon Materials for High-Efficiency Sodium Ion Storage. *Adv. Energy Mater.* **2017**, *7*, 1700403.
- (37) Li, Y.; Li, Y.; Pei, A.; Yan, K.; Sun, Y.; Wu, C. L.; Joubert, L. M.; Chin, R.; Koh, A. L.; Yu, Y.; Perrino, J.; Butz, B.; Chu, S.; Cui, Y. Atomic Structure of Sensitive Battery Materials and Analyses Revealed by Cryo–Electron Microscopy. *Science* **2017**, *358*, 506–510.
- (38) Xu, C.; Lindgren, F.; Philippe, B.; Gorgoi, M.; Björefors, F.; Edström, K.; Gustafsson, T. Improved Performance of the Silicon Anode for Li-Ion Batteries: Understanding the Surface Modification Mechanism of Fluoroethylene Carbonate as an Effective Electrolyte Additive. *Chem. Mater.* **2015**, *27*, 2591–2599.
- (39) Michan, A. L.; Parimalam, B. S.; Leskes, M.; Kerber, R. N.; Yoon, T.; Grey, C. P.; Lucht, B. L. Fluoroethylene Carbonate and Vinylene Carbonate Reduction: Understanding Lithium-Ion Battery Electrolyte Additives and Solid Electrolyte Interphase Formation. *Chem. Mater.* **2016**, *28*, 8149–8159.
- (40) Xu, G.; Wang, X.; Li, J.; Shangguan, X.; Huang, S.; Lu, D.; Chen, B.; Ma, J.; Dong, S.; Zhou, X.; Kong, Q.; Cui, G. Tracing the Impact of Hybrid Functional Additives on a High-Voltage (5 V-class) SiO_x-C/LiNi_{0.5}Mn_{1.5}O₄ Li-Ion Battery System. *Chem. Mater.* **2018**, *30*, 8291–8302.
- (41) Zhu, H.; Russell, J. A.; Fang, Z.; Barnes, P.; Li, L.; Efav, C. M.; Muenzer, A.; May, J.; Hamal, K.; Cheng, I. F.; Davis, P. H.; Dufek, E. J.; Xiong, H. A Comparison of Solid Electrolyte Interphase Formation and Evolution on Highly Oriented Pyrolytic and Disordered Graphite Negative Electrodes in Lithium-Ion Batteries. *Small* **2021**, *17*, 2105292.
- (42) Soto, F. A.; Yan, P.; Engelhard, M. H.; Marzouk, A.; Wang, C.; Xu, G.; Chen, Z.; Amine, K.; Liu, J.; Sprenkle, V. L.; El-Mellouhi, F.; Balbuena, P. B.; Li, X.; Soto, F. A.; Balbuena, P. B.; Yan, P.; Engelhard, M. H.; Wang, C.; Liu, J.; Sprenkle, V. L.; Li, X.; Marzouk, A.; El-Mellouhi, F.; Xu, G.; Chen, Z.; Amine, K. Tuning the Solid Electrolyte Interphase for Selective Li- and Na-Ion Storage in Hard Carbon. *Adv. Mater.* **2017**, *29*, 1606860.
- (43) Ma, L. A.; Naylor, A. J.; Nyholm, L.; Younesi, R. Strategies for Mitigating Dissolution of Solid Electrolyte Interphases in Sodium-Ion Batteries. *Angew. Chem., Int. Ed.* **2021**, *60*, 4855.